Journal of Materials Chemistry C

Accepted Manuscript

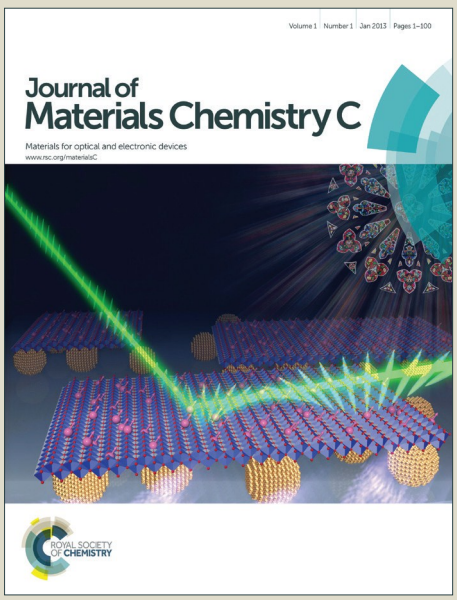

This is an *Accepted Manuscript*, which has been through the Royal Society of Chemistry peer review process and has been accepted for publication.

Accepted Manuscripts are published online shortly after acceptance, before technical editing, formatting and proof reading. Using this free service, authors can make their results available to the community, in citable form, before we publish the edited article. We will replace this *Accepted Manuscript* with the edited and formatted *Advance Article* as soon as it is available.

You can find more information about *Accepted Manuscripts* in the Information for Authors.

Please note that technical editing may introduce minor changes to the text and/or graphics, which may alter content. The journal's standard Terms & Conditions and the Ethical guidelines still apply. In no event shall the Royal Society of Chemistry be held responsible for any errors or omissions in this *Accepted Manuscript* or any consequences arising from the use of any information it contains.

ROYAL SOCIETY OF CHEMISTRY

www.rsc.org/materialsC

Journal Name

ARTICLE TYPE

Cite this: DOI: 10.1039/xxxxxxxxxx

Comparison of solution-mixed and sequentially processed P3HT:F4TCNQ films: effect of doping-induced aggregation on film morphology†

Ian E. Jacobs,[a] Erik W. Aasen,[a] Julia L. Oliveira,[a] Tayane N. Fonseca,[a] John D. Roehling,[b] Jun Li,[a] Gwangwu Zhang,[c] Matthew P. Augustine,[c] Mark Mascal,[c] and Adam J. Moulé[a,c*]

Received Date
Accepted Date

DOI: 10.1039/xxxxxxxxxx

www.rsc.org/journalname

Doping polymeric semiconductors often drastically reduces the solubility of the polymer, leading to difficulties in processing doped films. Here, we compare optical, electrical, and morphological properties of P3HT films doped with F4TCNQ, both from mixed solutions and using sequential solution processing with orthogonal solvents. We demonstrate that sequential doping occurs rapidly (<1 sec), and that the film doping level can be precisely controlled by varying the concentration of the doping solution. Furthermore, the choice of sequential doping solvent controls whether dopant anions are included or excluded from polymer crystallites. Atomic force microscopy (AFM) reveals that sequential doping produces significantly more uniform films on the nanoscale than the mixed-solution method. In addition, we show that mixed-solution doping induces the formation of aggregates even at low doping levels, resulting in drastic changes to film morphology. Sequentially coated films show 3-15 times higher conductivities at a given doping level than solution-doped films, with sequentially doped films processed to exclude dopant anions from polymer crystallites showing the highest conductivities. We propose a mechanism for doping induced aggregation in which the shift of the polymer HOMO level upon aggregation couples ionization and solvation energies. To show that the methodology is widely applicable, we demonstrate that several different polymer:dopant systems can be prepared by sequential doping.

Introduction

The discovery of the high conductivity of polyacetylene upon treatment with iodine vapor[1] was a seminal discovery in the field of organic electronics, and was cited by the Nobel committee in their award of the 2000 Nobel Prize in Chemistry. This treatment is called doping, in analogy to inorganic semiconductors. The purposes of doping are the same in organic materials; adjusting work function to control interface dipoles and controlling conductivity. Despite the similarities, however, the details differ significantly in organic materials. Dopants in organic semiconductors are materials with extremely high electron affinities (p-type dopants) or very low ionization potentials (n-type dopants). These can take the form of inorganic oxidizing or reducing agents, but in recent years neutral organic molecules, such as the strong electron acceptor 2,3,5,6-tetrafluoro-7,7,8,8-tetracyanoquinodimethane (F4TCNQ), and particularly the combination of regioregular poly-3-hexylthiophene (P3HT) and F4TCNQ (structures shown in Figure 1a), have become the focus of intense study.[2–8] Molecular dopants such as F4TCNQ undergo ground–state charge transfer with their host semiconductor, yielding polarons or bipolarons on the semiconductor.[5,8–15] The dopant anions remain in the film as counter-ions (radical anions in the case of F4TCNQ).

This process is relatively straightforward, however, details of the mechanism remain unclear. Although significant progress has been made in recent years, it is still in general difficult to predict whether a given semiconductor:dopant system will undergo integer or fractional charge transfer.[5,16–19] In addition, even in systems which show integer charge transfer, as is the case with P3HT:F4TCNQ, typically only a small proportion of the generated charges (∼5%) appear to contribute to charge transport.[5,8]

An additional challenge is the stability and processing of doped organic films. Because the dopant counter-ions are not covalently bonded to the organic semiconductor, they are free to diffuse

[a] Department of Chemical Engineering and Materials Science, University of California, Davis, California, USA; E-mail: amoule@ucdavis.edu
[b] Materials Science Division, Lawrence Livermore National Laboratory, 7000 East Ave. Livermore, CA 94550
[c] Department of Chemistry, University of California, Davis, California, USA.

† Electronic Supplementary Information (ESI) available: [details of any supplementary information available should be included here]. See DOI: 10.1039/b000000x/

Journal of Materials Chemistry C Accepted Manuscript

and/or drift under an applied electric field. For example, iodine, a popular dopant in early years of research on organic semiconductors, was abandoned in part due to its tendency to rapidly diffuse out of films or into other layers on time scales of minutes to hours. Such behavior is unacceptable for devices with desired lifetimes of years. Recent work has shown that even a relatively large molecular dopant like F4TCNQ (MW = 276 g/mol) can diffuse in small molecule and polymer semiconductor films below 80°C.[20–24] Several groups have synthesized and studied alternative molecular dopants in an effort to increase the thermal stability of doped films.[21,25–32]

Finally, a less commonly discussed but equally problematic issue lies in solution processing doped films. Several groups have noted that doping often results in drastically reduced solubility of polymers; as a result, mixed polymer:dopant solutions must be kept at high temperatures and dilute concentrations, and tend to rapidly aggregate, forming gels or large particles.[4,33,34] Unfortunately, increasing solution temperatures to prevent aggregation has been shown to reduce doping efficiency.[6] Such behavior is far too capricious for industrial applications.

In some cases, this reduction in solubility can be advantageous. Our group recently used F4TCNQ to demonstrate reversible solubility control on thin films of P3HT.[7] We showed that doped films are completely insoluble in organic solvents, but chemical or optical de-doping methods can recover intrinsic material properties. This method, called doping induced solubility control (DISC), can be used to stack mutually soluble materials or for sub-micron patterning. In developing this process we found that P3HT films could be doped with F4TCNQ by simply exposing coated P3HT films to a F4TCNQ solution in a solvent orthogonal to the polymer, such as acetonitrile. This method greatly simplifies the processing of doped films compared to the traditional mixed-solution method. A schematic of the two methods are shown in Figure 1b and 1d.

In this article, we compare the properties of films doped sequentially vs. the standard mixed-solution method. We observe that sequentially doped films are much easier to process, significantly less rough, and show higher conductivity at a given doping ratio, indicating increased carrier mobility, fewer trapped charge carriers, or some combination of the two. Sequential doping methods are fully compatible with roll-to-roll solution processing. In addition, we demonstrate sequential doping in several different polymer:dopant systems, showcasing the wide applicability of the process.

Results and Discussion

Doping Level Determination

Optical spectroscopy is well-suited for the characterization of doped films, due to sub-gap absorptions from polaronic species. Several types of charge carriers are known to exist in doped polymers, however, in recent work by Wang, et al., fits to optical spectra suggest singly-charged polarons are the dominant charge carrier in P3HT:F4TCNQ films.[8] Positive polarons give rise to two allowed sub-gap transition bands; in P3HT, these transitions occur at about 0.5 eV and 1.5 eV.[35,36] In addition, the F4TCNQ counter-ion shows sharp, distinctive absorption bands at 3.0, 1.8, 1.65, and 1.45 eV which match those of [K+][F4TCNQ$^{\bullet-}$] in solution (see Figure 1).

Figure 1b shows the typical mixed solution doping method: P3HT and F4TCNQ solutions in chlorobenzene (CB) are mixed and quickly spin coated to form a film. As illustrated and as will be demonstrated below, the addition of the dopant solution results in rapid aggregation of the polymer. As a result, mixing is typically performed at elevated temperatures and immediately before spin coating. This is the typical method of preparing polymer:F4TCNQ films in the literature.[4,5,8,13,14,18,19,25,33,34] Figure 1c shows UV-vis-NIR spectra of films prepared using the mixed solution method at doping levels between 0.5 and 17 mol% F4TCNQ. All spectra are normalized to 1 at the P3HT $\pi-\pi^*$ absorption max (~2.3 eV). As expected, as the F4TCNQ mole ratio is increased, absorption bands corresponding to the F4TCNQ$^{\bullet-}$ radical anion (3.0, 1.8, 1.6, and 1.45 eV) grow in, along with absorption bands at 0.5 and 1.5 eV corresponding to the P3HT$^{\bullet+}$ polaron and a corresponding bleach of the P3HT $\pi-\pi^*$ band at 2.3 eV. Our results show essentially complete bleaching of the P3HT $\pi-\pi^*$ band at a doping level of 17 mol%, consistent with previous reports.[4]

Figure 1d shows the sequential doping method. Here, undoped P3HT films are first spin coated from CB. Once dried, the films are doped on the spin coater by applying a solution of F4TCNQ and spinning off the excess solution. By varying the concentration and solvent of the F4TCNQ solution, the doping level can be precisely controlled. The corresponding UV-vis-NIR spectra are shown in Figure 1e.

Duong, et al. performed XRD studies of P3HT:F4TCNQ prepared by the mixed-solution method, and observed a new P3HT crystal structure above doping levels of about 3%, which was interpreted as intercalation of F4TCNQ into the polymer crystallites[4]. Because acetonitrile is a poor solvent for P3HT, and specifically because P3HT films show no solvochromic shift when immersed in acetonitrile,[7] very little solvent infiltration into crystalline polymer domains is expected. Therefore, we expect that only the disordered regions of the film are accessible to the dopant molecules, limiting the achievable doping level from an acetonitrile solution (or any poor solvent for P3HT).

Previous work[7] has also established that P3HT films are completely insoluble after sequential doping from a 0.1 mg/ml F4TNCQ / acetonitrile solution. Despite their insolubility, these films still show a significant solvochromic absorption shift in typically good solvents for P3HT, such as CB, indicating that solvent is able to infiltrate crystallites in the film without causing dissolution. This property can be exploited to reach higher doping levels: first, a P3HT film is doped with F4TCNQ using a 0.1 mg/ml acetonitrile solution, which renders the film insoluble. Then, the film is further doped from a more concentrated F4TCNQ solution in CB. As shown in Figure 1e, these films show significantly higher doping levels than those doped from an acetonitrile solution alone.

Because the doping levels of the mixed solution samples are known, we can use their UV-vis-NIR spectra to estimate the doping levels of the sequentially doped samples. Details of the fitting

Journal of Materials Chemistry C Accepted Manuscript

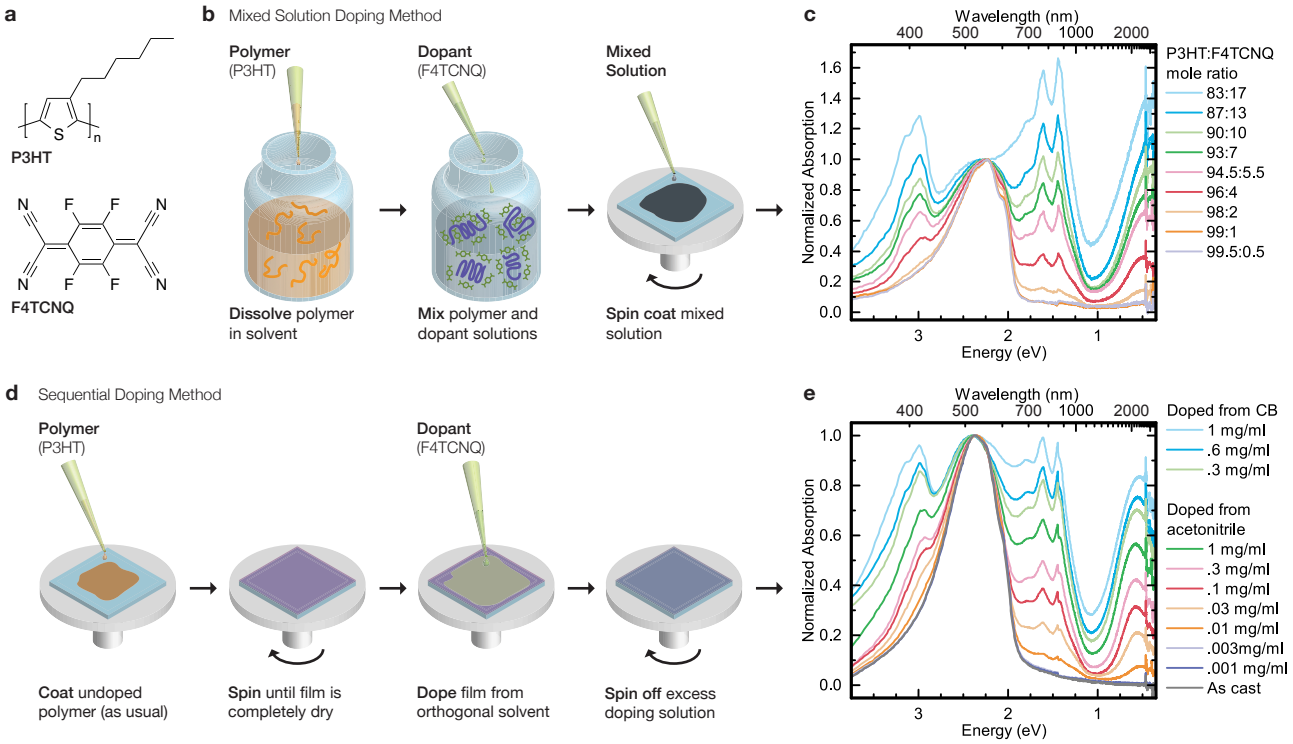

Fig. 1 Schematic of the two doping methods and corresponding UV-vis-NIR spectra of P3HT doped with F4TCNQ (molecular structures shown in (a)). In the mixed solution doping method (b), P3HT and F4TCNQ solutions are prepared in a common solvent, such as chlorobenzene (CB). These solutions are then mixed, generally resulting in aggregation, and then spin-coated to form a film. Corresponding UV-vis-NIR spectra at P3HT:F4TCNQ molar ratios from 99.5:0.5 to 83:17 are shown in (c). In the sequential doping method (d), intrinsic P3HT films are first spin-coated, then doped by F4TCNQ in acetonitrile (an orthogonal solvent). Varying the F4TCNQ solution concentration allows for control of film doping level; higher doping levels are achieved by first doping with F4TCNQ in 0.1 mg/ml acetonitrile followed by F4TCNQ in CB. The corresponding UV-vis-NIR spectra are shown in (e). Legend shows F4TCNQ acetonitrile solution concentration, while CB denotes films doped sequentially with F4TCNQ in CB.

are discussed in Supplemental Information section 1, but a brief overview is given here. All spectra were normalized to the maximum of the P3HT $\pi-\pi*$ band at 2.3 eV. Gaussians were then fit to the IR absorption band at 0.5-0.6 eV, generally attributed to the P1 polaron band of P3HT.[36] This band was chosen due to its relative isolation from other spectral features. A plot of the absorption maxima of this band yields two linear regions (between 0-4 mol% and 5.5-17 mol%), with a discontinuous intermediate region (Supplementary Figure 1). Such a discontinuity is not entirely unexpected when considered in the context of the previously reported F4TCNQ intercalation into the crystalline P3HT domains above 3 mol% doping.[4] These linear fits were then used to convert the IR absorption of the sequentially doped samples to estimated doping level, listed in Supplementary Tables 1 and 2.

With knowledge of the doping levels present in the sequentially doped films, we are able to perform a more quantitative analysis of the process. Figure 2a shows UV-vis-NIR spectra of an as-cast P3HT film, as well as films doped by exposure to a 0.1 mg/ml solution of F4TCNQ in acetonitrile for exposure times between 1 and 30 seconds. The extremely weak dependence on exposure time suggests the establishment of an equilibrium between the neutral F4TCNQ in the solvent and ionized F4TCNQ in the P3HT matrix. This equilibrium is clearly reached in much less than one second, indicating that this process could be easily incorporated into large-scale, roll-to-roll manufacturing processes.

Figure 2b shows film doping level as a function of doping solution concentration. The 'S' curve shape seen in the experimental data suggests a model for the equilibrium conditions must consider the finite number of doping sites available in the film. The simplest model incorporating this is the Langmuir isotherm model,[37] given by:

$$C_{d,sat} - C_d = \Theta = \frac{K_{eq}C_s}{1+K_{eq}C_s} \quad (1)$$

where C_d is the film doping level, $C_{d,sat}$ is the saturated film doping level which would be reached if doped with an infinitely concentrated solution, Θ is the proportion of occupied doping sites in the film, C_s is the concentration of the dopant in solution, and K_{eq} is the equilibrium constant.

Using K_{eq} and $C_{d,sat}$ as fit parameters, we can achieve good agreement with the experimental data. Assuming that the doping solution solvent used (acetonitrile) is capable of swelling amorphous P3HT domains but not crystalline domains, $C_{d,sat}$ should correspond to the solubility of F4TCNQ in the amorphous polymer domains (an assumption that we will verify in Figure 4, below). Our fit indicates $C_{d,sat}$ = 4.9 mol%. The extracted equilibrium constant is ~8000, corresponding to a ΔG of -0.23 eV for the reaction $F4TCNQ_{CH_3CN}$ + P3HT ⇌ $F4TCNQ^{\bullet-}_{P3HT}$ + $P3HT^{\bullet+}$.

Journal of Materials Chemistry C Accepted Manuscript

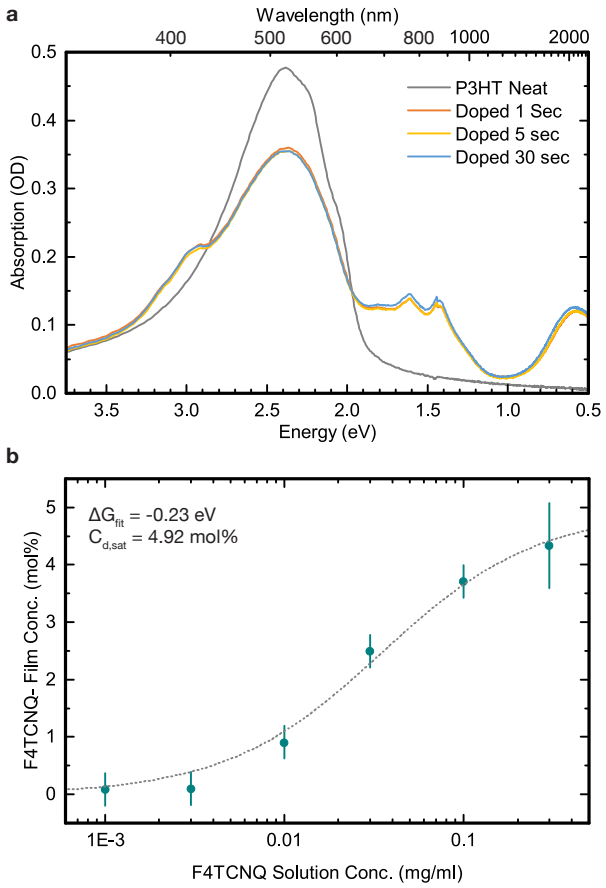

Fig. 2 Sequential doping exposure time dependence and fitting to Langmuir isotherm model. a) UV-vis-NIR spectra of P3HT films exposed to a 0.1 mg/ml solution of F4TCNQ in acetonitrile for times between 1 and 30 seconds. b) Film doping level (given as F4TCNQ- Film concentration) as a function of doping solution concentration. Data points are experimental data with doping level estimated by IR absorption; the dashed line is a fit to a Langmuir isotherm model. The extracted fit parameters are shown inset.

This value is in excellent agreement with the HOMO-LUMO offset of P3HT (HOMO = 5.0 eV)[25] and F4TCNQ (LUMO = 5.24 eV),[25] indicating that ionization is the primary driving force for solvation of F4TCNQ in the P3HT matrix.

Film Morphology

We now turn our attention to film morphology. Figure 3 shows atomic force microscopy images of films doped using the mixed solution process (a) and the sequential process (b). As is clearly visible in Figure 3a, the mixed-solution method yields significantly rougher films. Supplementary Figure 2 shows RMS roughness calculated from these images. Even doping at 0.5 mol% results in a doubling of RMS roughness compared to as-cast films, increasing to 2.9 nm from 1.3 nm.

In contrast, the sequentially doped films shown in Figure 3b show morphology essentially identical to as-cast up to the 0.1 mg/ml doped sample. No significant phase segregation is visible until the doping solution reaches 1 mg/ml, which reveals large clusters. These structures are almost certainly phase-segregated F4TCNQ domains, given the solubility limit of 4.9 mol% obtained from the fit in Figure 2b. However, the samples further doped from a CB solutions show very little phase segregation, as confirmed by the low roughness data (<1.5 nm RMS) for the CB doped samples shown in Figure S2. These observations suggest that doping from acetonitrile does not allow a significant fraction of F4TCNQ to infiltrate P3HT crystallites, and the 4.9 mol% solubility limit obtained previously corresponds to the solubility of F4TCNQ in amorphous P3HT domains. Doping from CB allows F4TCNQ to enter crystalline P3HT domains as expected, given the observed solvochromic shift seen in CB swelled P3HT:F4TCNQ films.[7] Therefore, sequential doping first from acetonitrile and then from CB allows the achievement of higher doping levels.

To verify whether doping from acetonitrile solution allows F4TCNQ to intercalate into P3HT crystallites, we measured electron diffraction patterns of undoped P3HT and three films with similar doping levels (3.7 mol%) but different preparation methods. Due to the preferred edge-on orientation of P3HT with respect to the substrate, the $\pi-\pi$ stacking diffraction peak is easily observed in the electron diffraction geometry.[38] However, due to the same preferred orientation and the larger lattice constant (corresponding to smaller diffraction angle), the (100) lamellar stacking peak is not typically observable.[38] As a result, we limit our analysis here to the $\pi-\pi$ stacking dimension only.

Radially integrated diffraction patterns showing the P3HT $\pi-\pi$ stacking dimension are shown in Figure 4. In previous work, XRD revealed a shift in both the P3HT $\pi-\pi$ stacking and lamellar stacking dimensions in P3HT:F4TCNQ mixed-solution films at doping levels above ~3 mol%.[4] These shifts were interpreted as resulting from F4TCNQ intercalation into P3HT crystallites. Examining our electron diffraction results in Figure 4, both undoped P3HT (Figure 4a) and P3HT:F4TCNQ doped from acetonitrile show identical $\pi-\pi$ stacking spacings of 0.39 nm. However, if we swell the crystalline domains of a film identical to the one in Figure 4b with CB, we observe a reduction in the $\pi-\pi$ stacking dimension to 0.38 nm. This slightly lower spacing matches what we observe in a mixed-solution film with the same doping level (Figure 4d), and is consistent with previous XRD studies.[4,39]

Together, these results indicate that doping from acetonitrile does not allow F4TCNQ to intercalate into P3HT crystallites. However, this film morphology is only kinetically stable. Holes generated by the doping reaction preferentially move to the crystalline regions due to their lower bandgap[13,14], generating an electric field which should pull dopant anions into the P3HT crystallites. When the crystallites are swollen with solvent, as is the case when doping from mixed solutions or sequentially from "good" solvents like CB, the F4TCNQ anions are able to infiltrate the crystallites. This result clearly indicates that careful choice of doping solution solvent allows for fine control of the location of the dopant counter-ion, which is expected to play a major role in the electrical properties of the film.

Journal of Materials Chemistry C Accepted Manuscript

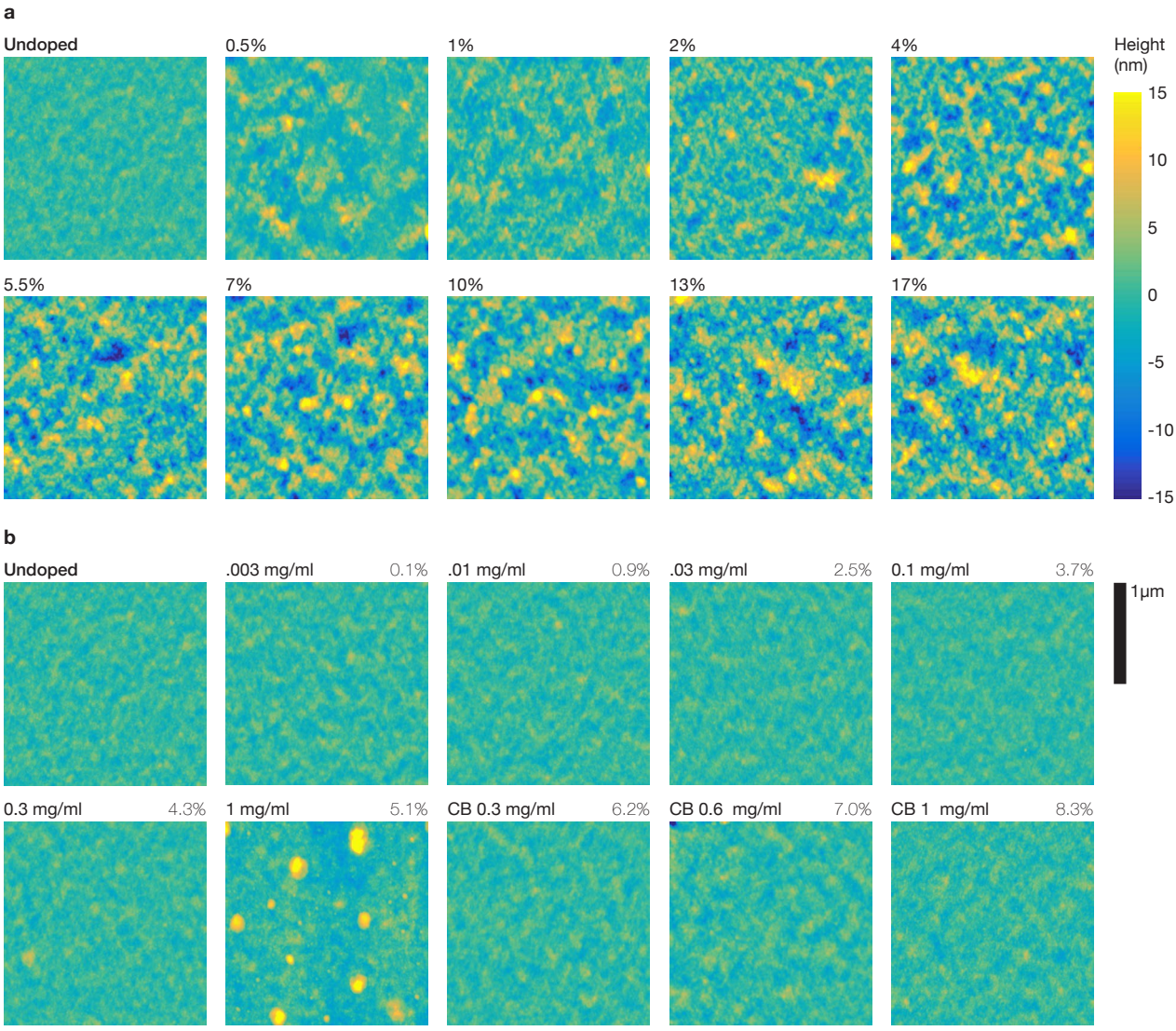

Fig. 3 Tapping mode AFM height images of F4TCNQ doped P3HT films using the mixed solution method (a), and the sequential method (b). Doping level of F4TCNQ in mol% is indicated above each image for mixed-solution films, while doping solution concentration is shown for sequentially doped films, along with doping level (in mol%) obtained from fits to IR absorption. Films doped sequentially from CB (as described previously) are labelled with CB before the solution concentration. All images are 2 μm square and plotted with the same height scale.

Morphological Development in Solution-mixed Films

The difficulty of processing mixed-solution samples, as well as the vast differences in film roughness between the sequential and mixed-solution doped samples, indicates that the mixed-solution samples are aggregating in solution. Figure 5 shows UV-vis spectra of a dilute P3HT solution (25 μg/ml in CB), undoped and with increasing mol% F4TCNQ. The broad absorption band at 2.75 eV (450 nm) is the unaggregated P3HT π-π^* absorption.[40] Upon aggregation, the P3HT absorption strongly red shifts and vibronic bands at 2.0 eV (0-0 transition) and 2.2 eV (0-1 transition) become resolved. The ratio of these two peaks is known to correlate to the degree of interchain order in P3HT,[41–44] and is also an indicator of the dominant type of excitonic coupling present: a 0-0 to 0-1 ratio of greater than unity corresponds to J-aggregation, while a ratio less than 1 corresponds to H-aggregation.[44] A spectrum of P3HT nanofibers (NFs) shows these bands clearly.[43–45] For comparison, a spectrum of P3HT J-aggregate NFs from ref. 38 is also included Figure 5.

As seen in Figure 5, the addition of F4TCNQ to the solution results in the growth of the same vibronic bands as seen in the NFs, along with a corresponding reduction in the unaggregated P3HT absorption. The similarity of doped polymer solution spectra to the nanofiber spectrum appears to indicate that doping induces the formation of crystalline nanoparticles. Because of the rapid change in solubility upon doping, we expect that the high nucleation rate would cause most of these particles to contain relatively few polymer chains, along with ionized dopant molecules.

Unfortunately, spectroscopy does not allow for a completely unambiguous assignment of the polymer nanostructure. The 0-0 to 0-1 vibronic peak ratios of $\sim$1 indicates these particles

Journal of Materials Chemistry C Accepted Manuscript

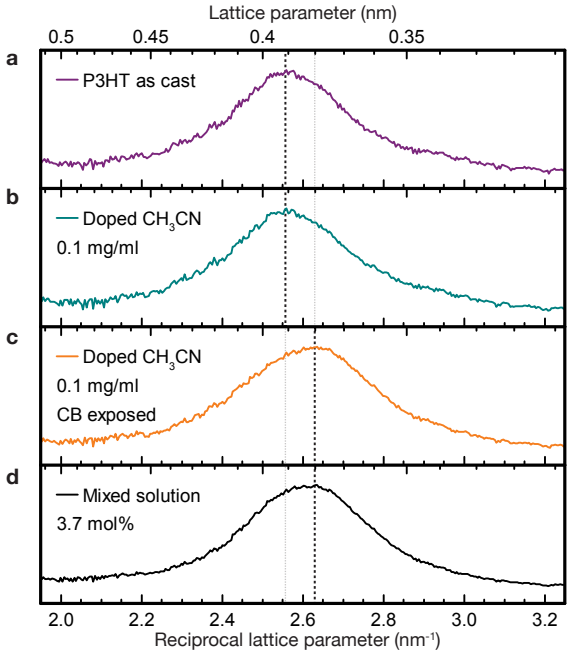

Fig. 4 Radially integrated electron diffraction patterns showing the P3HT $\pi - \pi$ stacking peak. Films (b-d) have similar doping levels, but different preparation methods. a) Undoped P3HT, b) P3HT:F4TCNQ sequentially doped from a 0.1 mg/ml acetonitrile solution, c) P3HT:F4TCNQ sequentially doped from a 0.1 mg/ml acetonitrile solution, wetted with ~50 μL CB and allowed to dry (approx. 10 minutes) and d) P3HT:F4TCNQ doped at 3.7 mol% prepared by the mixed solution method.

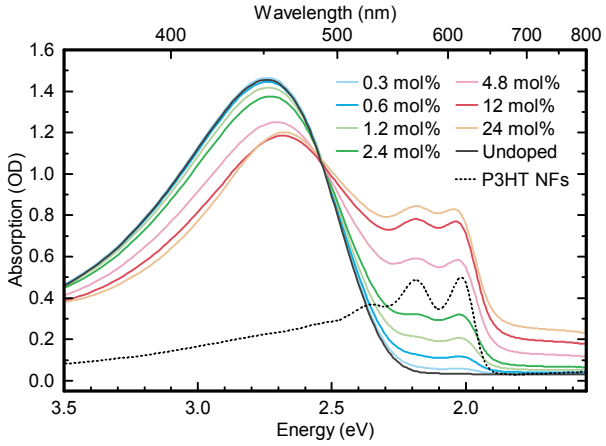

Fig. 5 UV-vis spectra of P3HT in CB (25 μg/ml) doped with varying amounts of F4TCNQ. The growth of peaks at 2.0 and 2.2 eV are indicative of aggregation, as can be seen by comparison with the spectra of undoped P3HT J-aggregate nanofibers (NFs) in suspension (~10 μg/ml in toluene).

show significant J-aggregate character. In work by Gao, et. al. on P3HT:F4TCNQ solutions[14], it was suggested that the presence of holes on the polymer backbone hinders rotation between the thiophene rings, allowing for single-chain J-aggregate coupling. In other words, it is possible that doped polymer chains could remain extended, but contain "stiff" sections which show J-aggregate properties as a result of the presence of polarons.

To further explore the nanostructure of P3HT doped in solution, weakly doped P3HT:F4TCNQ solutions (1 mg/ml P3HT, 1 mol% F4TCNQ) were dispersed onto glass substrates by spin coating. The spin coating speed (2500 rpm) was chosen so as to create a discontinuous film so individual particles could be imaged. We note that the solution concentration used (1 mg/ml) is typical for processing solution-mixed films, and thus should accurately illustrate the morphological development of the doped films studied elsewhere in this paper. Figure 6a shows a 10 μm square tapping mode AFM height image, revealing a highly discontinuous film composed of isolated particles and unconnected fibril-like structures. Higher resolution height and phase images of the area indicated in Figure 6a (red square) are shown in Figure 6b and 6c, respectively. Although the height image appears to show several seemingly continuous fibers surrounded by relatively bare substrate, the phase image reveals these structures are composed of smaller, relatively uniformly sized particles separated by clear grain boundaries. In addition, smaller, uniformly sized particles are visible dispersed throughout the image, even in areas which appear to be bare substrate in the height image. The size of these particles is consistent with nanoparticles formed from single polymer molecules. Clear discontinuities, visible at both the micron length scale visible in Figure 6a and the nanometer scale visible in Figure 6b-c, are consistent with the formation of isolated nanoparticles in solution.

Using the mixed-solution method with similar processing conditions, Duong et al. observed no change in P3HT crystal structure at doping levels below 3 mol%, indicating that at low dopant loadings, the $F4TCNQ^{\bullet -}$ are largely confined to amorphous domains. These results are confirmed in Supplementary Figure 3. In a dilute solution, then, we would expect the formation of positively charged, crystalline P3HT aggregates, surrounded by a shell of F4TCNQ anions. These particles would be expected to have a negative surface dipole and thus repel each other, which may explain the well-dispersed and uniformly-sized nanoparticles seen in the phase image (Figure 6c).

For comparison, Figures 6d-f show images of an undoped film processed and imaged identically to Figures 6a-c. This film is only ~2-3 nm thick, yet still is essentially continuous. At the larger length scales visible in Figure 6d, polymer islands appear to be well-connected. Higher resolution height and phase images (Figures 6e and f, respectively) clearly show connectivity between the islands visible in the larger image. The phase image (Figure 6f) also shows a well connected nanostructure, in clear contrast to the domain boundaries visible in the doped sample (Figure 6c). While it is easy to imagine how the morphology visible in the undoped film could lead to high conductivities, the drastically different morphology visible in the mixed solution doped samples does not appear to illustrate the development of a continuous percolation necessary for efficient charge transport.

Journal of Materials Chemistry C Accepted Manuscript

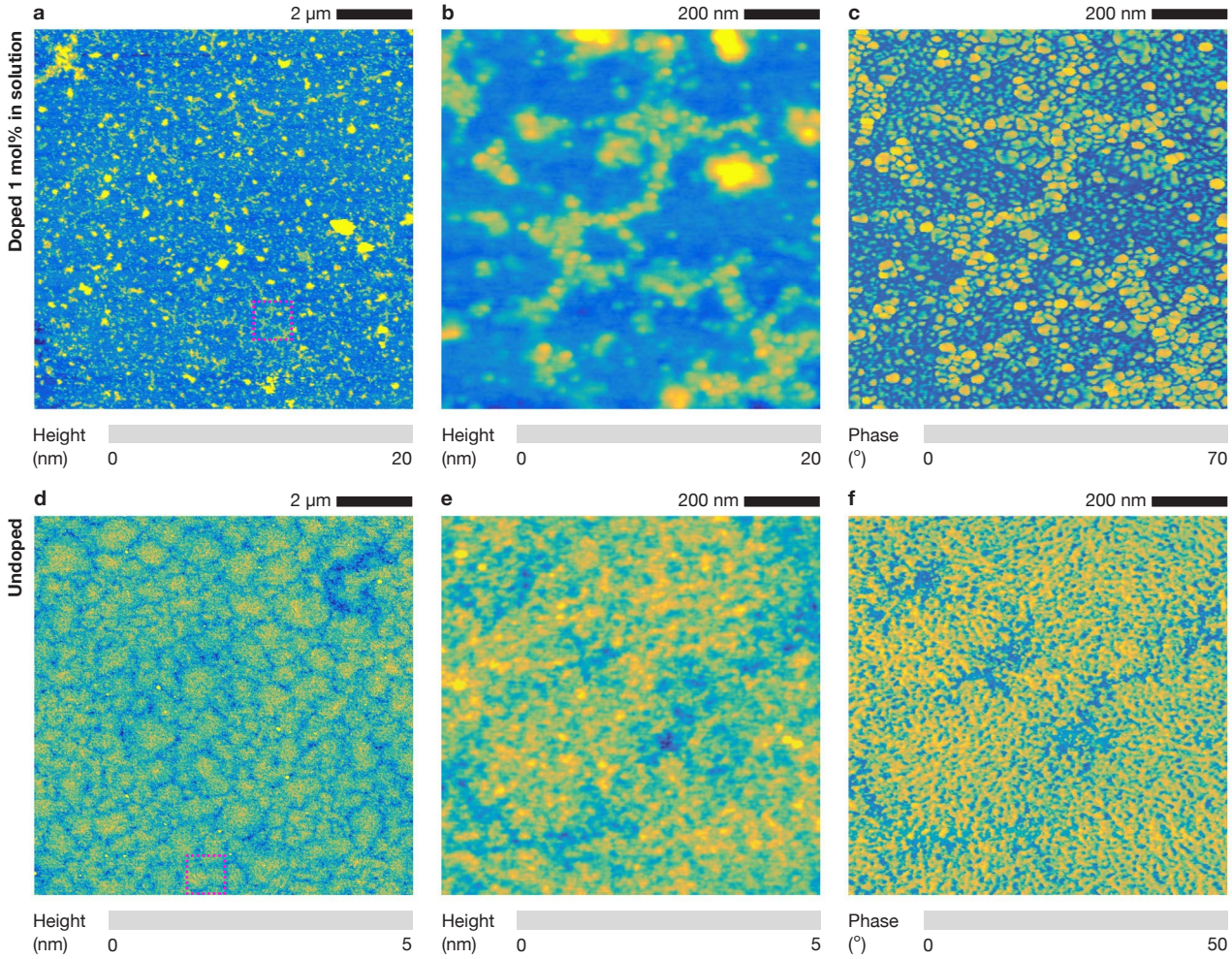

Fig. 6 Effect of aggregation on film morphology. Aggregate morphology was studied by spin coating a lightly doped P3HT:F4TCNQ solution (1 mg/ml in CB, doped 1 mol% F4TCNQ, 2500 rpm) onto a glass substrate to form a very thin, discontinuous film. Tapping mode AFM height imaging (a) reveals primarily isolated nanoparticles and some small fibril-shaped clusters. Detailed height (b) and phase (c) images of the area highlighted in (a) shows poor connectivity between domains in the fibril structures. For comparison, (d) shows an undoped P3HT film processed identically to (a-c), revealing an extremely thin but essentially continuous film. Here, detailed height (d) and phase (e) images of the area indicated in (d) show well-connected polymer domains. Note the difference in height scale between (a, b) and (d, e).

Solution Aggregation Mechanism

The work of Gao, et. al. suggests a mechanism by which doping could cause aggregation. In resonance Raman studies of doped thin films, the authors noted an increase in J-aggregate like spectral features which are indicative of significantly increased polymer backbone rigidity.[13] They concluded that F4TCNQ primarily injects holes into aggregated P3HT domains, and proposed that this is a result of a reduction in ionization potential of aggregates as compared to amorphous domains by approximately 0.3 eV.[13]. Our data suggests that this model is correct and by extension should explain aggregation in solution.

Assuming integer charge transfer, the driving force for ionization in a polymer:dopant system is given by the difference in energy between the polymer HOMO and the dopant LUMO. However, many polycrystalline polymers exhibit significant solvochromism, observed as a change in band gap between aggregated and solvated chains. The solvochromic effect can be seen in the spectra shown in Figure 5. For P3HT, the solvated chain bandgap is 2.75 eV, while the aggregated chain bandgap is 2.0 eV, giving the aforementioned HOMO level shift ΔHOMO_{agg} = -0.3 eV.

Consider now a single solvated polymer chain interacting with F4TCNQ in solution and neglecting any effects of solvent polarity. As the polymer doping level increases, the free energy of the aggregated state of the polymer chain is lowered relative to the solvated state by $\Delta G = C_d(\Delta\text{HOMO}_{agg} + \Delta G_{coulomb})$, where C_d is the doping level in mol% and $\Delta G_{coulomb}$ accounts for the coulomb repulsion that comes from adding an additional hole to the polymer. At low doping levels, we would expect $|\Delta\text{HOMO}_{agg}| > |\Delta G_{coulomb}|$ since ΔHOMO_{agg} = 0.3 eV, but $\Delta G_{coulomb}$ is proportional to doping level. In the limit that polarons are dilute (that is, $\Delta G_{coulomb}$ = 0), the expression above yields $\Delta G = -7.2$ kJ/mol per hole on the polymer. Therefore, addition of holes to the polymer will shift the equilibrium between solvated and aggregated states strongly

Journal of Materials Chemistry C Accepted Manuscript

in favor of aggregation. At higher doping levels, we would expect incorporation of dopant counter-ions into the crystalline domains to reduce $\Delta G_{coulomb}$ by charge screening, as experimentally observed in Figure 4 and in previous studies[4,6,39].

This mechanism explains several aspects of doping induced aggregation that are not accounted for by a shift in dielectric constant of the polymer:dopant system. First, doped polymers are generally insoluble in both non-polar and polar solvents. In addition, P3HT:F4TCNQ films show a solvochromic shift when swelled with typically good solvents for P3HT (such as CB), indicating solvent infiltration into crystalline polymer domains. If a shift in the polymer dielectric were responsible for insolubility, we would expect that solvents more polar than those which typically dissolve P3HT should also swell crystalline domains and as a result show a solvochromic shift. This behavior is not observed,[7] indicating that an increase in the dielectric constant is not the primary cause of reduced solubility in doped films.

Our mechanism indicates that in general, we should not expect significant dopant induced aggregation in amorphous polymers or crystalline materials that do not show significant solvochromaticity. In a study by Yim et al. on amorphous polyfluorenes doped with F4TCNQ, the authors note "doped solutions were clear with no precipitation, which allows for convenient solution processing through spin-coating to fabricate thin films (70-100 nm)."[19] In our lab, we also observe no reduction in the solubility of F8-PFB (one of the materials studied in Yim, et. al.) upon doping with F4TCNQ, despite a HOMO-LUMO offset of -0.15eV, which indicates that ionization should be exothermic.

However, there are other mechanisms by which doping may render amorphous or non-solvochromic polymers insoluble. Formation of nanoparticles in solution was observed by Parashchuk, et Al. in the poly[methoxy-5-(20-ethylhexyloxy)-1,4-phenylene-vinylene] (MEH-PPV) : 2,4,7-trinitrofluorenone (TNF) donor:acceptor system.[46,47] In the MEH-PPV:TNF system, it was proposed that fractional charge transfer complexes between the polymer and the acceptor mediate interactions between polymer chains in a manner analogous to a cross-linking reaction. However, this mechanism requires intercalation of the dopant into the polymer domains, which is inconsistent with previous observations that intercalation did not occur in P3HT:F4TCNQ at dopant loadings below ~3%, despite still causing a drastic reduction in solubility.[4] Supplemental Figure 3 verifies this: electron diffraction patterns of P3HT:F4TCNQ films doped at ~0.9 mol% show no change in $\pi-\pi$ stacking dimension, yet these films are still insoluble in CB. In addition, it is now well established that P3HT:F4TCNQ primarily undergoes integer charge transfer, and does not typically form charge transfer complexes.[5,8] It is therefore unlikely that the formation of fractional charge transfer complexes is responsible for the reduction in solubility of P3HT:F4TCNQ.

A 2009 study of MEH-PPV:F4TCNQ also indicated that at low doping ratios (1:600 dopant:polymer repeat unit), the addition of dopant "leads to the formation of aggregates immediately after mixing, resulting in unprocessable solutions."[34]. However, in this case the authors note that the cause appeared to be the low dielectric constant of the solvent (toluene, $\eta = 2.4$) and remedied

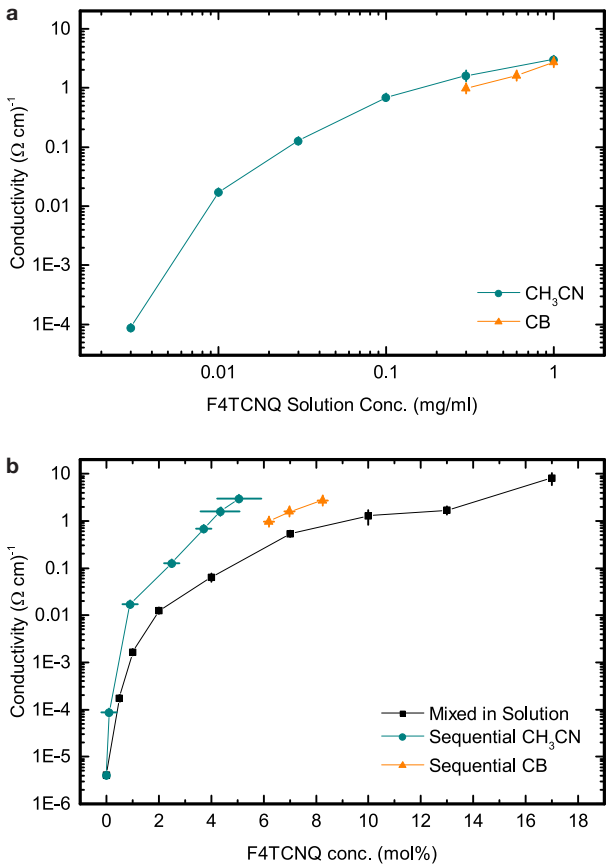

Fig. 7 a) Conductivity as a function of dopant solution concentration, and b) conductivity data of mixed-solution films vs. sequentially coated films, using doping levels derived from optical spectroscopy.

the issue by adding a small amount of a polar co-solvent. As discussed earlier, P3HT:F4TCNQ films are insoluble in solvents with a wide range of dielectric constants. Therefore, while a dielectric constant shift may play a role in doping induced aggregation for some polymer:dopant systems, it does not satisfactorily explain the insolubility of P3HT:F4TCNQ.

Conductivity in doped P3HT films

The doping-induced formation of nanoparticles in solution has strongly detrimental effects on the electrical properties of the resulting films. These issues are nicely avoided by sequential doping. Figure 7a shows the conductivity of films doped by the sequential method from F4TCNQ in acetonitrile, as well as films further doped from F4TCNQ in CB. As expected, increased doping solution concentration increases the film doping level, leading to conductivities controllable over more than 4 orders of magnitude, reaching a high conductivity of 3.0 S cm^{-1} for the 1 mg/ml CH_3CN sample. This conductivity is higher than previously reported for even highly doped (17 mol%) films mixed from solution,[4] however slightly lower than recent reports of sequentially doped films from THF:CH_2Cl_2.[39] Somewhat surprisingly, the films doped from CB solutions show slightly lower conductivity, despite their clearly higher doping levels as seen in the UV-vis-

Journal of Materials Chemistry C Accepted Manuscript

NIR spectra (Figure 1). The trend becomes more apparent when the data is replotted as a function of film doping level, shown in Figure 7b. Here, we demonstrate that at a given doping level, the sequentially doped films are considerably more conductive than solution-mixed films; using an acetonitrile doping solution, conductivity is higher by a factor between 5 and 15 between 1 and 5 mol% doping. Films doped from CB solutions are between 2.4 - 3.3 times as conductive as mixed-solution films. However, sequential doping limits the maximum achievable doping level. The 17 mol% mixed-solution film shows a conductivity of 8.0 S cm^{-1}, which to our knowledge is the highest reported conductivity for a P3HT:F4TCNQ film.

Conductivity in p-type doped films can be related to doping level by $\sigma = \mu_h e p$, where σ is conductivity, μ_h is the hole mobility, e is the elementary charge, and p is the density of mobile charge carriers. We can approximate p at doping levels well above the density of trap sites as $p = C_d \chi_I \chi_M$, where C_d is the density of dopant molecules in the film, χ_I is the mole fraction of dopant molecules that are ionized, and χ_M is the mole fraction of doping induced holes that are not trapped at any given time. The proportion of ionized dopant molecules is directly measurable by optical spectroscopy and has been reported to be on the order of 1.[5,8] This leaves mobility and χ_M as the two primary factors affecting conductivity.

Although relatively detailed models for energetic disorder and charge carrier mobility exist for P3HT,[17,48–51] these models do not capture the morphological subtleties from which these conductivity differences stem. Also, direct measurement of charge carrier mobility in doped films is difficult. Hall-effect mobilities of sequentially doped P3HT:F4TCNQ films were recently reported to be in the range of 0.003 to 0.02 $cm^2V^{-1}s^{-1}$.[39] Using the model given by Arkhipov, et al., between doping levels of $\sim$ 0.1 to 10%, coulombic traps from dopant counter-ions overlap and result in an increase in charge carrier mobility with respect to doping level of 3-4 orders of magnitude. However the majority of charge carriers are still expected to be trapped,[49] which is consistent with experimental results.[5] It is clear that neither charge carrier mobility nor the proportion of mobile carriers can be assumed to be constant. We therefore can only attribute the increased conductivities in the sequentially doped samples to an increase in the product $\mu_h \chi_M$ at a given doping level. Both of these factors could obviously be affected by morphology.

In recent work, Scholes, et al. used GIWAXS to show that in sequentially doped films, the polymer chains maintained the preferentially edge-on orientation seen in undoped P3HT.[39] This edge-on orientation with respect to the substrate puts the $\pi - \pi$ stacking direction in-plane, resulting in higher in-plane hole mobilities.[38] However, in mixed-solution films, Scholes et al. observed slightly more isotropic orientation of the polymer chains, which they reasoned was a result of solution-state aggregation.[39] This increase in anisotropy likely plays a role in the reduced conductivity observed in solution-mixed films. However, in the context of the vast morphological changes seen in Figure 6, the reduction in edge-on orientation appears to be one aspect of a larger problem: the reduction in connectivity between crystalline domains.

Given the morphological differences seen in Figure 6, we can interpret the conductivity data in the context of tie chains.[52] As shown in Figure 8a, our results thus far suggest mixed-solution films are composed of discrete, pre-formed crystallites with relatively few chains connecting them. As a result, we see a significant reduction in the mobility of charge carriers between crystallites, and also an increase in trapped charge carriers. In sequentially doped films (Figure 8b), morphology is set by the initial polymer spin coating, which creates a morphology with more tie chains between crystalline domains. Doping does not significantly change this morphology, allowing for higher conductivity at a given doping level.

Comparing the sequentially doped films from CB vs CH_3CN (Figure 7b), films doped from CB show higher doping levels without an increase in conductivity as compared to films doped from CH_3CN. This reduction in doping efficiency in CB doped samples implies the product $\mu_h \chi_M$ at a given doping level is lower for films doped from CB than from CH_3CN. On the other hand, as previously discussed, the Arkhipov model suggests that in this regime, mobility should increase as doping level increases. Assuming that mobility is predominantly determined by doping level, a reduction in χ_M, or in other words, an increase in the proportion of trapped charge carriers, would be responsible for the lower doping efficiency in CB doped films.

Both CB and CH_3CN doped films are initially cast from undoped P3HT, so the initial film morphology is identical. In addition, film roughness and surface topography after doping are essentially identical to as-cast for both CB and CH_3CN doped films. However, unlike in CH_3CN doped films, in CB doped samples we do expect significant incorporation of dopant counter-ions into the crystalline domains. Because the location of the dopant anion is expected to be the primary morphological difference between these samples, we conclude that segregation of dopant counter-ions and charge conduction pathways allows for higher conductivities at lower doping levels. This conclusion contradicts the results of some previous works,[4,6] which have suggested that incorporation of dopant molecules into polymer crystallites is a prerequisite for high doping efficiency.

Again, we can explain how the location of the dopant anion affects conductivity by the HOMO energy shift of the polymer. Dopant counter-ions can localize holes via coulombic interactions; however, if dopant counter-ions are segregated to amorphous domains, the increased HOMO level opposes the trapping potential, preventing the approach of holes from the crystalline domains. Incorporation of dopant ions into the crystal structure removes this barrier. Such complexities point to the need to incorporate morphological effects into models for doping in crystalline polymers, which has thus far been mostly glossed over.[17,48–51] At the same time, this model implies separation of dopant anions and charge carrier pathways via careful choice of sequential doping solvent and initial film morphology could allow for higher conductivities.

General applicability of sequential doping

In order to demonstrate the wide applicability of the sequential doping method, we also show that several other poly-

Journal of Materials Chemistry C Accepted Manuscript

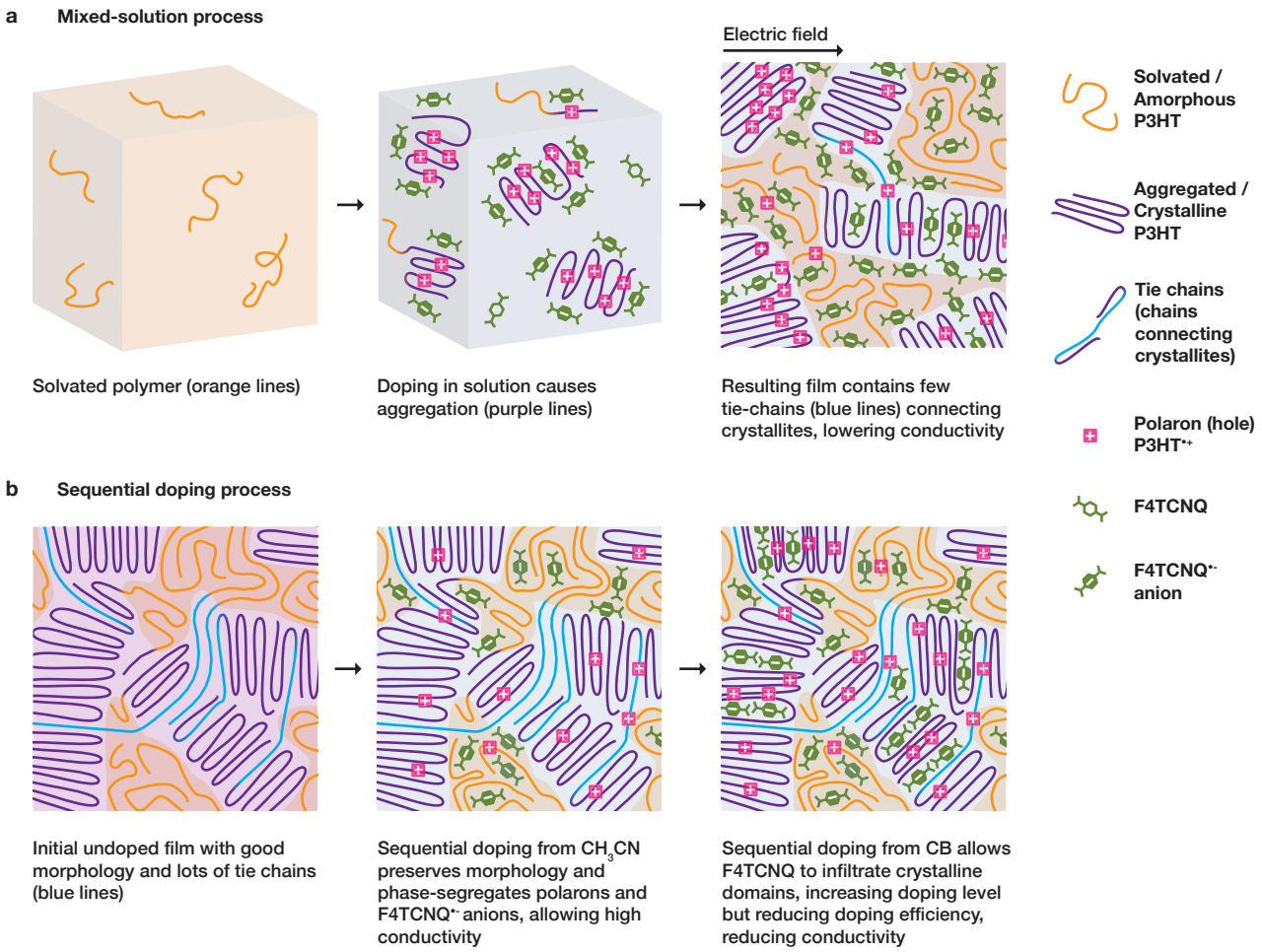

Fig. 8 Morphological development in mixed-solution and sequential doping. In the mixed-solution process (a), initially solvated P3HT aggregates in solution upon addition of F4TCNQ. When these aggregates are spun into a film, they form disconnected crystallites, with few tie chains (shown in blue). As a result, in an applied electric field, polarons cannot move easily between crystallites (shown upper right). The sequential process (b) avoids this issue since film morphology is set by initial film casting conditions. Doping from CH_3CN leaves F4TCNQ counter-ions only in amorphous domains, while polarons move to crystalline domains, allowing for unimpeded flow of charge. Doping from CB allows F4TCNQ anions to enter crystalline domains, increasing doping level but also the density of trap sites. As result, conductivity in CB doped films is slightly lower than CH_3CN doped films, despite their increased doping level.

mer:dopant systems that can be sequentially solution processed. Figure 9 shows UV-vis-NIR spectra and chemical structures of P3HT:F4OCTCNQ (a), P3HT:$Mo(tfd)_3$ (b), P3HT:DDQ (c) and PBTTT:F4TCNQ (d) prepared via the sequential method. All doped films show a clear bleach of the polymer $\pi - \pi*$ absorption band and polaron bands at ~1.5 eV and ~0.5 eV, clearly indicating doping. The effectiveness of the sequential doping method in the case of $Mo(tfd)_3$ is somewhat surprising, as it is considerably bulkier than the planar structure of F4TCNQ, and is only sparingly soluble in most common solvents.[29,30,32] These results suggest that sequential doping is widely applicable to other polymer:dopant systems.

In addition, after doping, these films are essentially insoluble in their casting solvents. The insolubility effect suggests a degree of universality to the mechanism of doping induced aggregation, as suggested by the discussion above. In the context of doping induced solubility control (DISC)–the use of molecular dopant to control solubility for multi-layer deposition and patterning–these results are promising.[7] They suggest that the DISC patterning process may be applicable to a wide range of dopant:polymer systems.

Conclusions

We have studied films of P3HT doped with F4TCNQ using solution mixed and sequential processing methods. Using the UV-vis-NIR spectra of the films, we show that doping level is tunable over a wide range by varying the doping solution concentration and quantified the doping level of the sequentially doped films. Sequential doping proceeds by rapid (<1 second) establishment of equilibrium between F4TCNQ solvation in the film and solution, following a simple Langmuir isotherm model. Fits to this model indicate that the solubility limit for F4TCNQ in amorphous P3HT domains is 4.9 mol%, and an activation energy for doping $\Delta G = -0.23$eV, is in good agreement with the HOMO-LUMO

Journal of Materials Chemistry C Accepted Manuscript

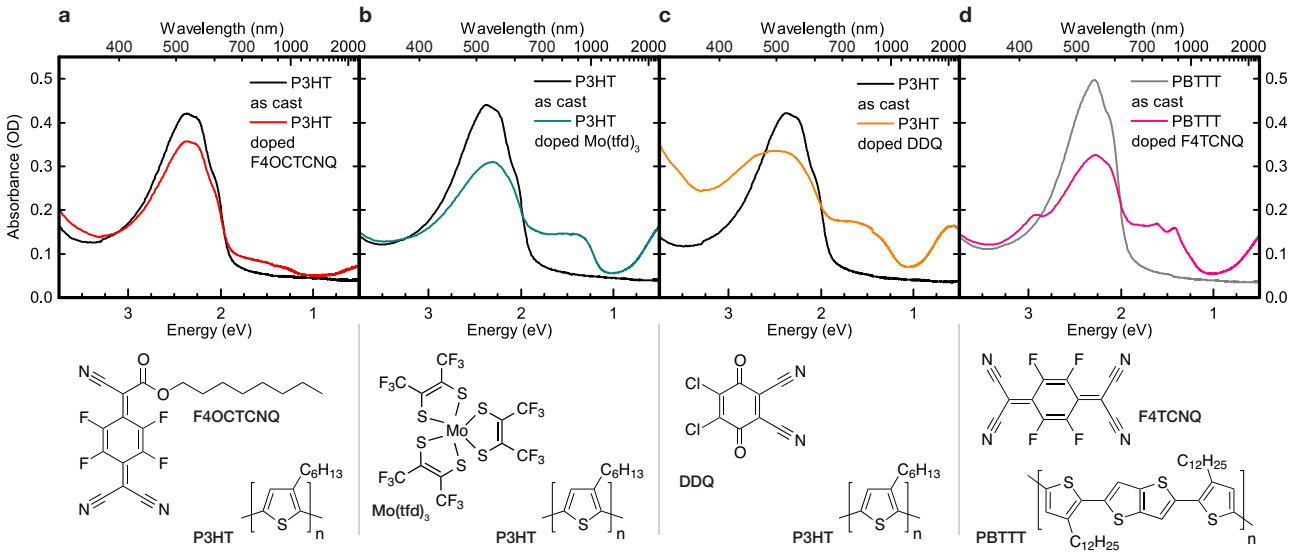

Fig. 9 Sequential doping applied to other polymer:dopant systems. a) P3HT:F4OCTCNQ, b) P3HT:$Mo(tfd)_3$, c) P3HT:DDQ, d) PBTTT:F4TCNQ. UV-vis-NIR spectra are shown above, while structures are shown below. Acetonitrile was used as the doping solvent for all systems. After doping, films are insoluble in their original casting solvent (CB).

offset of P3HT-F4TCNQ (−0.24 eV). These results indicate that incorporation of F4TCNQ into the P3HT films is primarily driven by ionization.

Atomic force microscopy reveals that sequentially doped films show morphology essentially identical to as-cast films. Mixed-solution preparation, on the other hand, produces considerably rougher films even at doping levels less than 1 mol%. Films doped from a poor solvent for P3HT (acetonitrile) show large, phase segregated domains at doping levels above the 4.9% solubility limit, while films doped from a good solvent for P3HT (chlorobenzene) show higher doping levels in optical spectra and no indication of phase segregation. Electron diffraction indicates that sequential doping from acetonitrile does not affect the P3HT $\pi - \pi$ spacing, but exposing these films to solvents able to swell P3HT crystallites allows F4TCNQ to intercalate into crystalline domains. Together, these results indicate that sequential doping solvent choice allows for control over whether the dopant counter-ions reside in amorphous or crystalline polymer domains.

Low concentration solution-state UV-vis-NIR indicates that doping induces aggregation in solution. AFM images of films cast from dilute doped solutions are discontinuous and appear to be formed form discrete polymer nanoparticles. We hypothesize that in doped solutions, P3HT crystals are surrounded by a shell of dopant ions, creating a negative surface dipole. As a result, doped particles repel each other and form discontinuous polymer domains when cast into films. We propose that doping may induce aggregation based on the HOMO level shift of the polymer upon aggregation.

When aggregated solutions are spun cast, the resulting films are composed of highly conductive doped crystalline domains, but these regions are not well connected by tie chains. As a result, conductivity is limited by the high electrical resistance between the conductive crystallites. By comparison, sequentially doped films have a large number of tie molecules between doped crystalline domains because these were formed before addition of the dopants. The improved morphology of the sequentially doped films means that conductivity is higher than mixed-solution films by a factor of 5 to 15 at the same doping level. In addition, films doped sequentially from acetonitrile followed by chlorobenzene solutions do not show higher conductivity than films doped from acetonitrile, despite higher doping levels, indicating that incorporation of dopant anions into crystalline domains decreases the proportion of mobile charge carriers. The correlation of counter-ion location with material properties suggests that to achieve high-conductivity doped polymer films, conductive pathways and dopant counter-ions should be spatially separated.

Lastly, we demonstrate that the sequential doping process is applicable to a range of different dopant molecules and polymers, and that doping induced aggregation appears to be a universal trend, at least in crystalline polymer:dopant systems. This suggests that sequential doping may enable the engineering of enhanced electrical characteristics in other systems as well.

Methods

Materials

P3HT (Plextronics, MW = 65 kDa), PBTTT-C12, and DDQ were purchased from Sigma-Aldrich. F4TCNQ was purchased from TCI (98+%). F4OCTCNQ was synthesized as described previously.[25] $Mo(tfd)_3$ was provided by the Marder group (Georgia Institute of Technology).[29] PEDOT:PSS (Clevios P VP AI 4083) was purchased from Heraeus. Solvents were purchased from Sigma-Aldrich and dried over 3A molecular sieves; all other materials were used as received.

Journal of Materials Chemistry C Accepted Manuscript

Sample preparation

P3HT (10 mg/ml, CB) and F4TCNQ (1 mg/ml CB) solutions were heated to 60°C and left to dissolve overnight. F4TCNQ solutions in acetonitrile used for sequential doping were prepared at room temperature shortly before use. One-inch glass slides (Fisher Scientific) for UV-vis-NIR spectroscopy and AFM and silicon substrates for conductivity testing were cleaned by sequential sonication steps in acetone, 10% Mucasal:DI water, and DI water, dried with nitrogen, and UV-ozone treated for 30 minutes before use. All sample preparation was performed in a nitrogen glovebox (<3 ppm H_2O, O_2) equipped with a molecular sieve solvent trap.

Mixed-solution doping

Before use, P3HT solutions were diluted with CB and kept at 60°C. Immediately before spin coating, P3HT solutions were mixed with F4TCNQ at 60°C to give solutions between 1 and 2 mg/ml P3HT. Concentrations and spin coating speeds were varied to obtain approximately 50 nm thick films.

Sequential doping

Thin films of P3HT were prepared by spin coating P3HT (10mg/ml, CB) to form approximately 50 nm thick films. Doping was performed by wetting the film with F4TCNQ (various conc., CH_3CN), waiting 5 seconds, then spinning off the excess solution at 1000 rpm. Films doped from CB solutions were prepared by first doping with F4TCNQ in acetonitrile (0.1 mg/ml) to render the films insoluble, then doping from CB solution following the same procedure.

Conductivity samples

Samples for conductivity measurements were prepared as described above on silicon substrates (n-type (100), 300 nm oxide layer) photolithographically patterned with gold electrodes (5 nm Cr / 95 nm Au) with in a 4 point measurement design. Electrode width was 5mm and channel lengths were 1mm. Three samples per composition were measured.

TEM samples

Samples for transmission electron microscopy were prepared by first spin coating PEDOT:PSS (2500 rpm, ∼50 nm film thickness) through 0.2 μm syringe filters onto clean glass substrates. After heating to 110°C for 5 minutes in air, these PEDOT-coated substrates were transferred to the glovebox for sample prep as described above. These films were then floated off the substrates in water, and collected on a TEM grid (Ted Pella) for imaging.

Characterization

UV-vis-NIR spectroscopy was performed on a Perkin-Elmer Lambda 750. Solution-state measurements were collected in 10 mm path length quartz cuvettes. Atomic force microscopy was carried out in tapping mode on a Digital Instruments Multimode AFM with phase extender module, using BudgetSensor TAP-300G probes. Conductivity measurements were performed in the dark under nitrogen (<3 ppm H_2O, O_2), using a Keithley 2420 sourcemeter. Voltage drops at multiple current source values were collected to ensure ohmic behavior. Radial intensity diffraction patterns were collected on a JEOL 2000 FX microscope at 200 kV and radially integrated in MATLAB. The beam current and intensity were kept as low as possible to minimize beam damage. No degradation of the diffraction pattern could be observed after several minutes of illumination on the same area.

Acknowledgments

This research project was supported by the U.S. Department of Energy, Office of Basic Energy Sciences, Division of Materials Sciences and Engineering, under Award No. DE-SC0010419. This work was also performed in part under the auspices of the U.S. Department of Energy (DOE) by Lawrence Livermore National Laboratory under Contract DE-AC52-07NA27344. J.L.O. (CAPES Scholar No. 88888.038733/2013-00) and T.N.F. (CAPES Scholar No. 88888.039070/2013-00) would like to acknowledge the support of CAPES Foundation, Ministry of Education of Brazil, Brasília - DF 70040-020, Brazil. The authors would also like to thank the group of Seth Marder for providing the $Mo(tfd)_3$ sample, Joseph Sit and Ray Hickey for assistance with TEM sample preparation, and Thomas Harrelson helpful discussion.

References

1 H. Shirakawa, E. J. Louis, A. G. MacDiarmid, C. K. Chiang and A. J. Heeger, *J. Chem. Soc., Chem. Commun.*, 1977, 578–580.
2 L. Ma, W. H. Lee, Y. D. Park, J. S. Kim, H. S. Lee and K. Cho, *Applied Physics Letters*, 2008, **92**, 063310.
3 L. Zhu, E.-G. Kim, Y. Yi and J.-L. Brédas, *Chemistry of Materials*, 2011, **23**, 5149–5159.
4 D. T. Duong, C. Wang, E. Antono, M. F. Toney and A. Salleo, *Organic Electronics*, 2013, **14**, 1330–1336.
5 P. Pingel and D. Neher, *Physical Review B*, 2013, **87**, 115209–.
6 D. T. Duong, H. Phan, D. Hanifi, P. S. Jo, T.-Q. Nguyen and A. Salleo, *Advanced Materials*, 2014, **26**, 6069–6073.
7 I. E. Jacobs, J. Li, S. L. Burg, D. J. Bilsky, B. T. Rotondo, M. P. Augustine, P. Stroeve and A. J. Moulé, *ACS Nano*, 2015, **9**, 1905–1912.
8 C. Wang, D. T. Duong, K. Vandewal, J. Rivnay and A. Salleo, *Physical Review B*, 2015, **91**, 085205–.
9 M. Pfeiffer, A. Beyer, T. Fritz and K. Leo, *Applied Physics Letters*, 1998, **73**, 3202–3204.
10 W. Gao and A. Kahn, *Applied Physics Letters*, 2001, **79**, 4040–4042.
11 X. Zhou, M. Pfeiffer, J. Blochwitz, A. Werner, A. Nollau and T. Fritz, *Applied Physics Letters*, 2001, **78**, 410–412.
12 S. Braun and W. R. Salaneck, *Chemical Physics Letters*, 2007, **438**, 259–262.
13 J. Gao, J. D. Roehling, Y. Li, H. Guo, A. J. Moule and J. K. Grey, *Journal of Materials Chemistry C*, 2013, **1**, 5638–5646.
14 J. Gao, E. T. Niles and J. K. Grey, *The Journal of Physical Chemistry Letters*, 2013, **4**, 2953–2957.
15 J. Gao, B. W. Stein, A. K. Thomas, J. A. Garcia, J. Yang, M. L. Kirk and J. K. Grey, *The Journal of Physical Chemistry C*, 2015, **119**, 16396–16402.
16 H. Mendez, G. Heimel, S. Winkler, J. Frisch, A. Opitz, K. Sauer,

Journal of Materials Chemistry C Accepted Manuscript

B. Wegner, M. Oehzelt, C. Rothel, S. Duhm, D. Tobbens, N. Koch and I. Salzmann, *Nat Commun*, 2015, **6**, year.

17 I. Salzmann, G. Heimel, S. Duhm, M. Oehzelt, P. Pingel, B. M. George, A. Schnegg, K. Lips, R.-P. Blum, A. Vollmer and N. Koch, *Physical Review Letters*, 2012, **108**, 035502–.

18 H. Méndez, G. Heimel, A. Opitz, K. Sauer, P. Barkowski, M. Oehzelt, J. Soeda, T. Okamoto, J. Takeya, J.-B. Arlin, J.-Y. Balandier, Y. Geerts, N. Koch and I. Salzmann, *Angewandte Chemie*, 2013, **125**, 7905–7909.

19 K.-H. Yim, G. L. Whiting, C. E. Murphy, J. J. M. Halls, J. H. Burroughes, R. H. Friend and J.-S. Kim, *Advanced Materials*, 2008, **20**, 3319–3324.

20 J. Li, C. W. Rochester, I. E. Jacobs, S. Friedrich, P. Stroeve, M. Riede and A. J. Moulé, *ACS Applied Materials & Interfaces*, 2015, **7**, 28420–28428.

21 R. Meerheim, S. Olthof, M. Hermenau, S. Scholz, A. Petrich, N. Tessler, O. Solomeshch, B. Lüssem, M. Riede and K. Leo, *Journal of Applied Physics*, 2011, **109**, 103102.

22 P. Tyagi, S. Tuli and R. Srivastava, *The Journal of Chemical Physics*, 2015, **142**, 054707.

23 J. Huang, M. Pfeiffer, A. Werner, J. Blochwitz, K. Leo and S. Liu, *Applied Physics Letters*, 2002, **80**, 139–141.

24 J. Li, C. W. Rochester, I. E. Jacobs, E. W. Aasen, S. Friedrich, P. Stroeve and A. J. Moule, *Organic Electronics*, 2016.

25 J. Li, G. Zhang, D. M. Holm, I. E. Jacobs, B. Yin, P. Stroeve, M. Mascal and A. J. Moulé, *Chemistry of Materials*, 2015, **27**, 5765–5774.

26 C.-C. Chang, M.-T. Hsieh, J.-F. Chen, S.-W. Hwang and C. H. Chen, *Applied Physics Letters*, 2006, **89**, 253504.

27 Z. Q. Gao, B. X. Mi, G. Z. Xu, Y. Q. Wan, M. L. Gong, K. W. Cheah and C. H. Chen, *Chemical Communications*, 2008, 117–119.

28 B. X. Mi, Z. Q. Gao, K. W. Cheah and C. H. Chen, *Applied Physics Letters*, 2009, **94**, 073507.

29 Y. Qi, T. Sajoto, S. Barlow, E.-G. Kim, J.-L. B. , S. R. Marder and A. Kahn, *Journal of the American Chemical Society*, 2009, **131**, 12530–12531.

30 Y. Qi, T. Sajoto, M. Kröger, A. M. Kandabarow, W. Park, S. Barlow, E.-G. Kim, L. Wielunski, L. C. Feldman, R. A. Bartynski, J.-L. Brédas, S. R. Marder and A. Kahn, *Chemistry of Materials*, 2010, **22**, 524–531.

31 I. Bruder, S. Watanabe, J. Qu, I. B. Müller, R. Kopecek, J. Hwang, J. Weis and N. Langer, *Organic Electronics*, 2010, **11**, 589–593.

32 A. Dai, Y. Zhou, A. L. Shu, S. K. Mohapatra, H. Wang, C. Fuentes-Hernandez, Y. Zhang, S. Barlow, Y.-L. Loo, S. R. Marder, B. Kippelen and A. Kahn, *Advanced Functional Materials*, 2014, **24**, 2197–2204.

33 J. E. Cochran, M. J. N. Junk, A. M. Glaudell, P. L. Miller, J. S. Cowart, M. F. Toney, C. J. Hawker, B. F. Chmelka and M. L. Chabinyc, *Macromolecules*, 2014, **47**, 6836–6846.

34 Y. Zhang, B. de Boer and P. W. M. Blom, *Advanced Functional Materials*, 2009, **19**, 1901–1905.

35 R. Österbacka, C. P. An, X. M. Jiang and Z. V. Vardeny, *Science*, 2000, **287**, 839–842.

36 O. J. Korovyanko, R. Österbacka, X. M. Jiang, Z. V. Vardeny and R. A. J. Janssen, *Physical Review B*, 2001, **64**, 235122–.

37 I. Langmuir, *Journal of the American Chemical Society*, 1918, **40**, 1361–1403.

38 Z. Bao, A. Dodabalapur and A. J. Lovinger, *Applied Physics Letters*, 1996, **69**, 4108–4110.

39 D. T. Scholes, S. A. Hawks, P. Y. Yee, H. Wu, J. R. Lindemuth, S. H. Tolbert and B. J. Schwartz, *The Journal of Physical Chemistry Letters*, 2015, **6**, 4786–4793.

40 M. M. Bouman, E. E. Havinga, R. A. J. Janssen and E. W. Meijer, *Molecular Crystals and Liquid Crystals Science and Technology. Section A. Molecular Crystals and Liquid Crystals*, 1994, **256**, 439–448.

41 J. Clark, C. Silva, R. H. Friend and F. C. Spano, *Physical Review Letters*, 2007, **98**, 206406–.

42 F. C. Spano, *Accounts of Chemical Research*, 2010, **43**, 429–439.

43 J. D. Roehling, I. Arslan and A. J. Moule, *Journal of Materials Chemistry*, 2012, **22**, 2498–2506.

44 E. T. Niles, J. D. Roehling, H. Yamagata, A. J. Wise, F. C. Spano, A. J. Moulé and J. K. Grey, *The Journal of Physical Chemistry Letters*, 2012, **3**, 259–263.

45 K. J. Ihn, J. Moulton and P. Smith, *Journal of Polymer Science Part B: Polymer Physics*, 1993, **31**, 735–742.

46 O. D. Parashchuk, V. V. Bruevich and D. Y. Paraschuk, *Physical Chemistry Chemical Physics*, 2010, **12**, 6021–6026.

47 O. D. Parashchuk, T. V. Laptinskaya and D. Y. Paraschuk, *Physical Chemistry Chemical Physics*, 2011, **13**, 3775–3781.

48 V. I. Arkhipov, P. Heremans, E. V. Emelianova and H. Bässler, *Physical Review B*, 2005, **71**, 045214–.

49 V. I. Arkhipov, E. V. Emelianova, P. Heremans and H. Bässler, *Physical Review B*, 2005, **72**, 235202–.

50 V. I. Arkhipov, P. Heremans, E. V. Emelianova, G. J. Adriaenssens and H. Bässler, *Applied Physics Letters*, 2003, **82**, 3245–3247.

51 V. I. Arkhipov, P. Heremans, E. V. Emelianova, G. J. Adriaenssens and H. Bässler, *Journal of Physics: Condensed Matter*, 2002, **14**, 9899.

52 R. Noriega, J. Rivnay, K. Vandewal, F. P. V. Koch, N. Stingelin, P. Smith, M. F. Toney and A. Salleo, *Nat Mater*, 2013, **12**, 1038–1044.

Journal of Materials Chemistry C Accepted Manuscript

Mixed Solution Doping

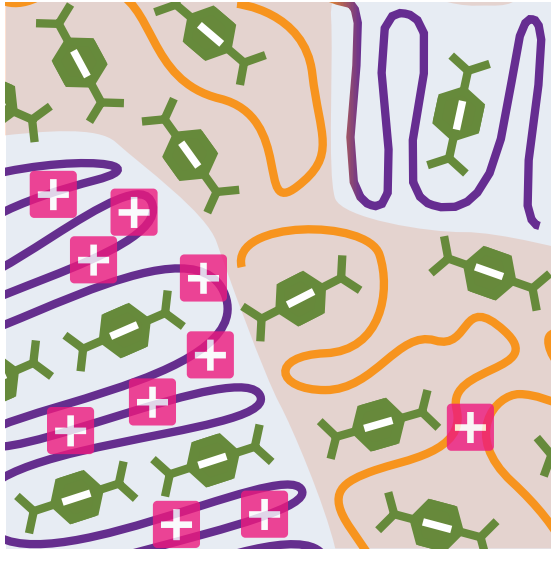

✗ Poor connectivity

✗ Intercalated dopants

→ Reduced conductivity

Sequential Doping

Neutral doping solvent

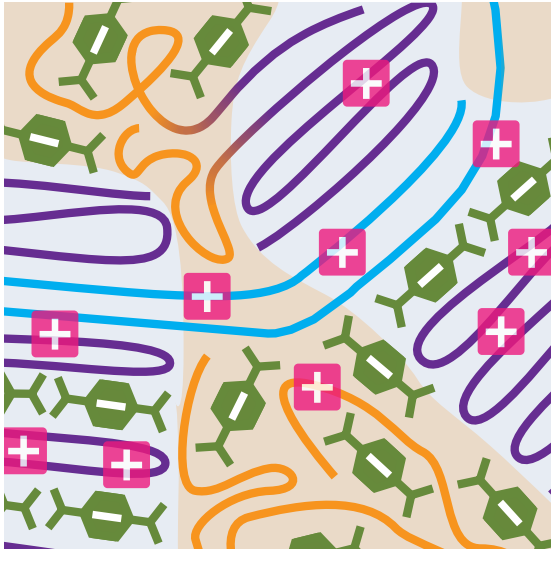

✓ Good connectivity

✗ Intercalated dopants

→ 3x higher conductivity

Doping solvent

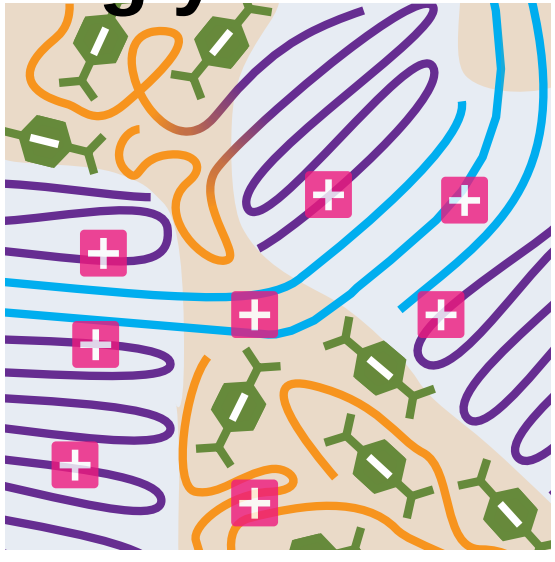

✓ Good connectivity

✓ Phase segregated dopants

→ 5-15x higher conductivity

Journal of Materials Chemistry C Accepted Manuscript